

Significant improvement of the self-protection capability of ultra-high temperature ceramic matrix composites

*Original*

Significant improvement of the self-protection capability of ultra-high temperature ceramic matrix composites / Servadei, F.; Zoli, L.; Vinci, A.; Galizia, P.; Sciti, D.. - In: CORROSION SCIENCE. - ISSN 0010-938X. - ELETTRONICO. - 189:(2021), p. 109575. [10.1016/j.corsci.2021.109575]

*Availability:*

This version is available at: 11583/2948360 since: 2022-01-21T10:19:44Z

*Publisher:*

Elsevier Ltd

*Published*

DOI:10.1016/j.corsci.2021.109575

*Terms of use:*

This article is made available under terms and conditions as specified in the corresponding bibliographic description in the repository

*Publisher copyright*

Elsevier postprint/Author's Accepted Manuscript

© 2021. This manuscript version is made available under the CC-BY-NC-ND 4.0 license  
<http://creativecommons.org/licenses/by-nc-nd/4.0/>. The final authenticated version is available online at:  
<http://dx.doi.org/10.1016/j.corsci.2021.109575>

(Article begins on next page)

# Corrosion Science

## Significant improvement of the self-protection capability of ultra-high temperature ceramic matrix composites --Manuscript Draft--

<b>Manuscript Number:</b>	
<b>Article Type:</b>	Full Length Article
<b>Keywords:</b>	ceramic matrix composites; scanning electron microscopy field-emission; energy dispersive X-ray diffraction; Oxidation resistance; surface passivation
<b>Corresponding Author:</b>	Luca Zoli, Ph.D CNR-ISTEC Faenza, ITALY
<b>First Author:</b>	Francesca Sevadei, Dr.
<b>Order of Authors:</b>	Francesca Sevadei, Dr.
	Luca Zoli, Ph.D
	Antonio Vinci, Ph.D
	Pietro Galizia, Ph.D
	Diletta Sciti, Ph.D
<b>Abstract:</b>	<p>The oxidation behaviour of Cf/ZrB<sub>2</sub>-SiC with different fibre architecture, manufactured by slurry impregnation and polymer infiltration and mild pyrolysis, was investigated. Short term oxidation tests in air were performed for 1 and 5 min at 1500 and 1650 °C in a bottom loading furnace. Microstructure, oxide scale thickness and composition were analysed by SEM/EDS/XRD. Results indicated that a good dispersion of ZrB<sub>2</sub> particles in the polymer derived SiC(O) matrix promoted the formation of a compact scale filling surface holes left by fibre oxidation. 20-30 vol% of ZrB<sub>2</sub> in the material was found a good compromise between lightness and oxidation resistance.</p>

## Highlights

- Short term oxidation tests at 1500 and 1650 °C were carried out on C/ZrB<sub>2</sub>-SiC CMC
- Less than 30 vol.% of ZrB<sub>2</sub> into SiC(O) matrix is able to impart a fast passivation
- Oxidation resistance was affected by the distribution of ZrB<sub>2</sub> into the SiC matrix

## **Significant improvement of the self-protection capability of ultra-high temperature ceramic matrix composites**

Francesca Servadei

*CNR-ISTEC, Institute of Science and Technology for Ceramics, Via Granarolo 64, I-48018 Faenza, Italy*  
[francesca.servadei@istec.cnr.it](mailto:francesca.servadei@istec.cnr.it)

Luca Zoli\*

*CNR-ISTEC, Institute of Science and Technology for Ceramics, Via Granarolo 64, I-48018 Faenza, Italy*  
[luca.zoli@istec.cnr.it](mailto:luca.zoli@istec.cnr.it)

Antonio Vinci

*CNR-ISTEC, Institute of Science and Technology for Ceramics, Via Granarolo 64, I-48018 Faenza, Italy*  
[antonio.vinci@istec.cnr.it](mailto:antonio.vinci@istec.cnr.it)

Pietro Galizia

*CNR-ISTEC, Institute of Science and Technology for Ceramics, Via Granarolo 64, I-48018 Faenza, Italy*  
[pietro.galizia@istec.cnr.it](mailto:pietro.galizia@istec.cnr.it)

Diletta Sciti

*CNR-ISTEC, Institute of Science and Technology for Ceramics, Via Granarolo 64, I-48018 Faenza, Italy*  
[diletta.sciti@istec.cnr.it](mailto:diletta.sciti@istec.cnr.it)

*\*Author to whom correspondence should be addressed: [luca.zoli@istec.cnr.it](mailto:luca.zoli@istec.cnr.it)*

### **Abstract**

The oxidation behaviour of  $C_f/ZrB_2$ -SiC with different fibre architecture, manufactured by slurry impregnation and polymer infiltration and mild pyrolysis, was investigated. Short term oxidation tests in air were performed for 1 and 5 min at 1500 and 1650 °C in a bottom loading furnace.

Microstructure, oxide scale thickness and composition were analysed by SEM/EDS/XRD. Results indicated that a good dispersion of  $ZrB_2$  particles in the polymer derived SiC(O) matrix promoted the formation of a compact scale filling surface holes left by fibre oxidation. 20-30 vol% of  $ZrB_2$  in the material was found a good compromise between lightness and oxidation resistance.

**Keywords:** ceramic matrix composites, scanning electron microscopy field-emission, energy dispersive X-ray diffraction, oxidation resistance, surface passivation

## 1. Introduction

The impelling demand for components able to withstand harsh conditions has been an important driving force for continuous search of materials possessing always more challenging properties. Currently used thermal protection systems and rocket motor components of hypersonic space vehicles, satellite launchers (e.g. VEGA, ARIANE) and brake systems of hyper speed vehicles such as Formula 1 cars are made of ceramic matrix composites and carbon matrix composites (CMC and CAMCs, respectively). Recently, other sectors such as aviation and metallurgy are replacing refractory metals with CMCs and CAMCs.

On one hand carbon/carbon (C/C) composites have excellent high-temperature strength, low CTE and deformability, good thermal shock resistance. On the other hand they suffer of poor oxidation resistance (above 500 °C) and low wear resistance that reduce durability and restrict their applications in air at elevated temperature [1]. Carbon fibre-reinforced silicon carbide (C/SiC) composites possess most of the good properties of C/C composites, and in addition a better oxidation resistance because the diffusion of oxygen can be limited by the formation of a highly viscous film of silica [2,3]. However, the capability to protect carbon fibres is not effective in a wide range of conditions of temperature and heat fluxes [4–9].

In the past few years, borides and carbides of the early transition metals (group IV and V), so called ultra-high temperature ceramics (UHTC), have gained increasing interest to realize a new class of ultra-high temperature ceramic matrix composite materials for their excellent thermal and chemical stabilities [10–13]. Among the UHTCs,  $\text{ZrB}_2$  is the most investigated UHTC phase [13–15] because of balanced characteristics, such as relative low density ( $\sim 6 \text{ g/cm}^3$ ), good oxidation and

ablation resistance especially when combined with minor amount of other ceramic phases, such as SiC [16–18], La<sub>2</sub>O<sub>3</sub> [19,20] and TaSi<sub>2</sub> [21]. Such multiphase matrices offer a better oxidation resistance and self-healing capability in a wider range of temperatures of individual phase matrices indeed. For instance, the oxidation of pure ZrB<sub>2</sub> forms porous solid ZrO<sub>2</sub> and a film of liquid B<sub>2</sub>O<sub>3</sub>, which spreads on the surface and inhibits the inward diffusion of oxygen into the bulk underlying material (slowing fibre oxidation) up to its temperature of vaporization (~1100 °C). Conversely, a ZrB<sub>2</sub> - SiC matrix protect fibres also at higher temperature forming a borosilicate glass above 1100 °C, which is less viscous than pure silica, spreading better along the surface, sealing cracks and defects but at the same time is more viscous and less volatile than pure B<sub>2</sub>O<sub>3</sub> [22]. Moreover above 1600 °C ZrO<sub>2</sub> improves glass durability (solid particles embedded into the glass induce a physical modification) while its partial dissolution promote a chemical modification of Si-O bonds [23]. Consequently, the achievement of a homogeneous distribution of ZrB<sub>2</sub> and SiC phases around carbon fibres is the goal for improving material durability. Unfortunately, the phase composition (ceramic phases and carbon fibres) and their distribution in the composite are often the consequence of the manufacturing process selected rather than a study of the material design. Some examples of manufacturing method and characterization of oxidation resistance of UHTCMCs are reported in Table 1.

Table 1. Main results that have been done in this field of ceramic matrix composites and tests at high temperature to evaluate oxidation resistance.

Techniques	Materials	Fibre (vol%)	UHTC (vol%)	SiC (vol%)	Testing	Authors
PIP, VSI	C/C+ZrB <sub>2</sub> -SiC coating	n/a	n/a	n/a	Furnace, 1500 °C, 40 min	Zhou et al. [24]
CVI, PC	C/C+ZrB <sub>2</sub> -SiO <sub>2</sub> coating	n/a	n/a	n/a	Furnace, 1500 °C, 330 h	Haibo et al. [25]
CVI	C/C+ZrB <sub>2</sub> -SiC coating	n/a	n/a	n/a	Solar furnace, 1700–2600 °C	Corral et al. [26]
CVI	C/SiC-ZrB <sub>2</sub>	25	4	71	Electric furnace, 1000–1400 °C, 5 min	Tang et al. [27]
PIP, SI, CVD	C/ZrB <sub>2</sub> -SiC	54	n/a	n/a	Blow torch, 3000 °C, 20 s	Liu et al. [28]

SI, HP	C/ZrB <sub>2</sub> -SiC	42	52	6	TGA	Vinci et al. [29]
SI, HP	C/ZrB <sub>2</sub> -SiC	37	46	12	Furnace, 1500 and 1650 °C, 1 min	Vinci et al. [30]
SI, HP	C/ZrB <sub>2</sub> -SiC	53	26	17	Furnace, 1650 °C, 1 min	Zoli et al. [31]
SI, PIP	C/ZrB <sub>2</sub> -SiC	30-31	29-19	35-42	Furnace, 1650 °C, 1 min	Servadei et al. [33]
SI, PIP	C/ZrB <sub>2</sub> -SiC	30-31	29-19	35-42	TGA, furnace, 1500-1650 °C, 1-5 min	Present work

PIP: Polymer Infiltration and Pyrolysis.

VSI: Vapour Silicon Infiltration.

CVI: Chemical Vapour Infiltration.

PC: Pack Cementation.

SI: Slurry Infiltration.

CVD: Chemical Vapour Deposition.

HP: Hot Pressing.

Some authors applied an environmental barrier coating (EBC), made of UHTCs, on conventional C/C composites [24–26] and tested the material from 1500 to 2600 °C. The adhesion between the composite and the coating could be compromised due to the different chemistry of the materials and the thermal expansion mismatch under severe thermal stresses. Other authors introduced ZrB<sub>2</sub> powders into fibre preforms via slurry impregnation and consolidated the material using non-sintering routes: chemical vapour infiltration (CVI) with methane gas [27], polymer infiltration and pyrolysis (PIP) with polycarbosilane [28,32–34] and sintering approaches: pack cementation (PC) [25] and hot pressing (HP) [29–31].

Recently, we presented a novel two-step non-sintering near-net shape route to manufacture lightweight UHTCMCs (densities of 2.7 - 3.2 g/cm<sup>3</sup>) containing about 20 - 30 vol% of ZrB<sub>2</sub> (depending on fibre architecture) with homogeneous distribution of ZrB<sub>2</sub> and SiC phases around each carbon fibre, even using 2D cloths [32]. Even though the matrix was consolidated under the mild conditions of 1000 °C, passivation occurred within few microns below the material surface after oxidation at 1650 °C for 1 min [32].

Here we presented a deep investigation of the oxidation behaviour of the same material via thermogravimetric analysis (TGA) up to 1350 °C and short oxidation tests in air at 1500 and 1650 °C for 1 and 5 min. The aim of this work is to highlight that a good dispersion of ZrB<sub>2</sub> particles in the polymer derived SiC(O) matrix is to promote a fast passivation of the material.

## 2. Experimental

### 2.1 Materials

Commercially available products were used for the preparation of ceramic matrix composites, I) ceramic powders: SiC (Alpha, Grade UF-25, H.C. Starck, Germany; specific surface area 23–26 m<sup>2</sup>/g, impurities (wt.%): 2.6 O), ZrB<sub>2</sub> (Grade B, H.C. Starck, Germany; specific surface area 1.0 m<sup>2</sup>/g, particle size range 0.5–6 µm, impurities (wt.%): 2 O, 0.25 C, 0.25 N, 0.1 Fe, 0.2 Hf); II) polymeric precursor of SiC (Allyl-hydrido polycarbosilane, StarPCS<sup>TM</sup> SMP-10, Starfire System Inc., U.S.A.; density 0.998 g/cm<sup>3</sup>, viscosity 40–100 cPs at 25 °C) and the cross-linker catalyst (trimethyl(methylcyclopentadienyl)platinum(IV), Sigma Aldrich; purity 98%); III) unidirectional (UF-XN80-300, Granoc, Japan; fabric areal weight 330 g/m<sup>2</sup>) and plain woven (PF-XN80-240, Granoc, Japan; areal weight 240 g/m<sup>2</sup>) made of ultra-high modulus pitch-based carbon fibre (XN80-60S, yarn: 6K, diameter 10 µm, density 2.17 g/cm<sup>3</sup>, tensile modulus 780 GPa, tensile strength 3.4 GPa).

### 2.2 Process

Three C<sub>f</sub>/ZrB<sub>2</sub>-SiC samples with different fibre architecture were fabricated by a cycle of water-based slurry infiltration of fibre fabrics, using a mixture of ZrB<sub>2</sub> – 10 vol% SiC powders according to previous studies [31] followed by repetitive cycles of polymer infiltration and pyrolysis. A sample was realized by stacking infiltrated plain woven fabrics (sample labelled as 2D); a second sample, with an asymmetric orientation of fibres, was prepared by stacking unidirectional infiltrated fabrics with the same orientation (sample labelled as 0-0°), while a third sample, with symmetric configuration of fibres, was obtained by stacking unidirectional infiltrated



fabrics with 0-90° orientation (sample labelled as 0-90°). Infiltration with SMP-10 (containing 1 wt.% of catalyst) and pyrolysis cycles at 1000 °C under argon flux were carried out six times to reduce the porosity below 10%. Further details are reported in [32].

## 2.3 Oxidation tests

Regular samples sized 9 mm × 4 mm × 2 mm were cut from the pellet labelled 0-0°. In order to identify the critical oxidation temperatures, the oxidation test was carried out in a thermogravimetric analyser (STA 449 C Jupiter, NETZSCH, Geraetebau GmbH, Germany), in synthetic air (composition: 80 vol% N<sub>2</sub> + 20 vol% O<sub>2</sub>, with 30 mL/min gas flow), up to 1350 °C with a heating rate of 10 °C/min.

In order to evaluate resistance in extreme environments, short term oxidation tests were carried out in a bottom loading furnace (FC18-0311281, Nannetti S.r.l., Italy) at 1500 and 1650 °C in air for 1 and 5 min on 10 mm × 10 mm × as-processed thickness mm plates, which were cut from 0-0°, 0-90° and 2D samples. The plates were put on a porous zirconia sample holder, resting on one of the two largest surfaces, and introduced in the furnace when the target temperature was reached. At the end of the oxidation stage, the samples were removed and left to cool naturally in air.

## 2.4 Characterization

After the pyrolysis cycles, bulk densities were measured by the Archimedes' method. Open porosity in the range 0.0058-100 µm was determined by mercury intrusion porosimetry (Pascal 140 and Pascal 240 series, Thermo Finnigan, U.S.A.). The fibre volumetric amount was determined taking into account number of layers, sample area, the fibre areal weight (g/m<sup>2</sup>) and the fibre density given by the supplier. The powder amount in the matrix was calculated as the difference between the weight of the pellet after slurry infiltration (after drying) and fibre weight. The polymer derived ceramic weight was calculated as the difference between pellet weight after and before six PIP cycles. The topological characterization of the surface of the as-obtained samples was

performed with a Contour GT-K 3D non-contact profilometer (Bruker, Germany) on  $8 \times 8 \text{ mm}^2$  areas, then the data were analysed using the commercial software Vision64 Map.

Specimens for both oxidation tests were cleaned with ethanol and dried under IR lamp. During TGA test, the mass variation was recorded continuously by the analyser (sensitivity  $10^{-3} \text{ mg}$ ). Specimens for short oxidation tests were weighed with an analytical balance (accuracy  $\pm 0.01 \text{ mg}$ ) before ( $w_{\text{in}}$ ) and after oxidation test ( $w_{\text{fin}}$ ). Mass variation was normalized over the initial surface area using equation:  $\frac{\Delta m}{S} = \frac{w_{\text{fin}} - w_{\text{in}}}{S}$ , in which  $S$  is the initial surface area, measured by calliper (accuracy  $\pm 0.05 \text{ mm}$ ). X-ray diffraction analysis was carried out from  $10$  to  $80^\circ$  (step  $0.02$ , step time  $0.5 \text{ s}$ ) using an apparatus with  $\text{CuK}\alpha$  radiation (D8 Advance, Bruker, Germany) on air-exposed surface of samples to determine phases after oxidation. The microstructures and elemental composition of the as-processed material and oxidized specimens were analysed using field emission gun-scanning electron microscope (FE-SEM, Carl Zeiss Sigma NTS GmbH, Germany) and energy dispersive X-ray spectroscopy (EDS, INCA Energy 300, Oxford instruments, UK) on surface and cross-section, to reveal modifications induced by oxidation. Polished specimens for microscopy were prepared by cutting cross sections from tested samples, mounting them in epoxy resin and polishing them using semi-automatic polishing machine (Tegramin-25, Struers, Italy), then washed with ethanol and acetone in an ultrasonic bath. All oxidized samples were coated with a thin layer of carbon using a turbo-pumped sputter coater (Q150T ES, Quorum Technologies Ltd, UK).

### 3. Results and discussion

#### 3.1 Microstructure of as-obtained materials

In Table 2 the physical properties of samples UD ( $0-0^\circ$  and  $0-90^\circ$ ) presented in the previous work [32] and 2D are shown. Composition of matrix, amount of fibres and porosity were similar for unidirectional cloth reinforced samples regardless of fibre orientation on the plane. In the case of

2D sample a lower amount of  $\text{ZrB}_2$  phase, a higher amount of silicon carbide and a higher porosity were found.

Table 2. Bulk density, open porosity and compositions of the as-obtained composites [32].

Sample label	0-0°	0-90°	2D
Bulk density ( $\text{g/cm}^3$ )	$3.2 \pm 0.2$	$3.2 \pm 0.2$	$2.7 \pm 0.3$
Porosity (%)	~6	~6	~9
$C_f$ (vol%)	$30 \pm 1$	$31 \pm 1$	$30 \pm 1$
UHTC (vol%)	$29 \pm 1$	$27 \pm 1$	$19 \pm 1$
SiC (vol%)	$35 \pm 1$	$36 \pm 1$	$42 \pm 1$

Such differences in composition were ascribed to the higher complexity of fibre architecture of plain woven cloth (2D) compared to unidirectional cloth (UD). 2D cloths hindered the powder slurry infiltration more than UD cloths indeed. Moreover, the lower powder fraction in the infiltrated cloths explained also the lower UHTC content in the consolidated material offset by higher content of polymer derived ceramic (PDC). The higher number of defects in the powder/fibre compact was easily reduced by repetitive cycles of PIP due to the use of higher amount of low viscous SMP-10 [32]. The resulting 2D sample presented a higher roughness than UD samples. In Fig. 1a,b, the optical picture and the roughness profile mapping of 2D sample were reported. The Fig. 1b shows the shape and depth of four cavities formed at the intersection of the bundles on the external layer, and the 3D surface topography of two cavities were reported in Fig. 1c. Finally, the SEM analysis of the sample cross section highlighted the presence of PDC spots showing shape and size similar to the cavities visible on the sample surface, see Fig. 1d.

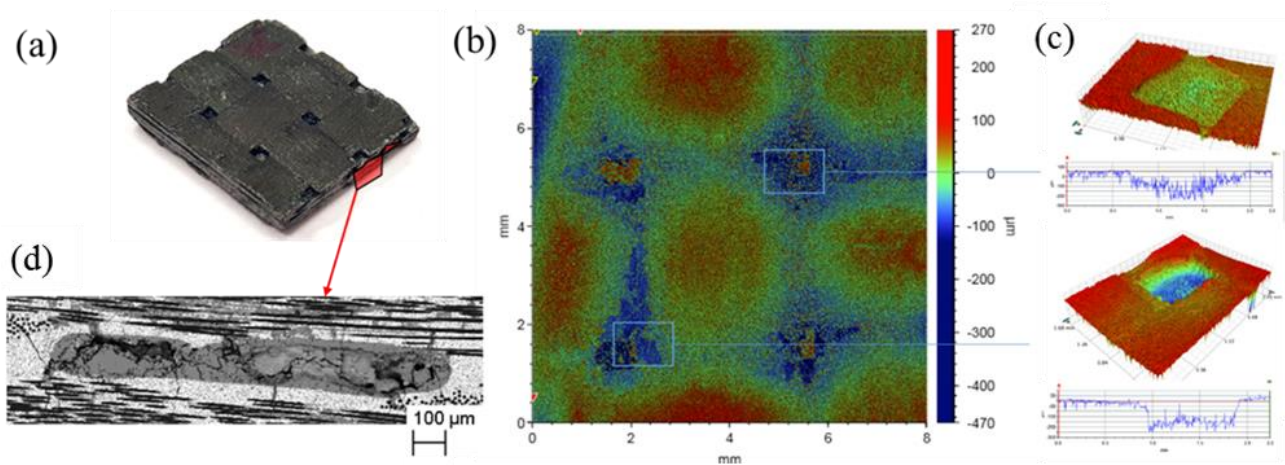


Figure 1. Sample 2D: (a) optical picture, (b) 2D image obtained by laser profilometer, (c) 3D detail of two areas of (b) showing surface topography, (d) back-scattering micrograph of cross section showing a PDC spot (grey colour) in the cross of fibre bundles.

Apart from above mentioned differences in sample compositions and porosities, the microstructures of the three samples were quite similar. An example of microstructure of the cross section of samples is shown in Fig. 2. Black dots are carbon fibres, the white contrasting phase is  $\text{ZrB}_2$ , while the grey regions are silicon carbide. Polymer derived ceramic (PDC) SiC was hardly distinguishable from SiC powder in Fig. 2 due to the low contrast between them, however the large spot of grey phase was PDC. Mainly,  $\text{ZrB}_2$  and SiC particles were well distributed around carbon fibres.

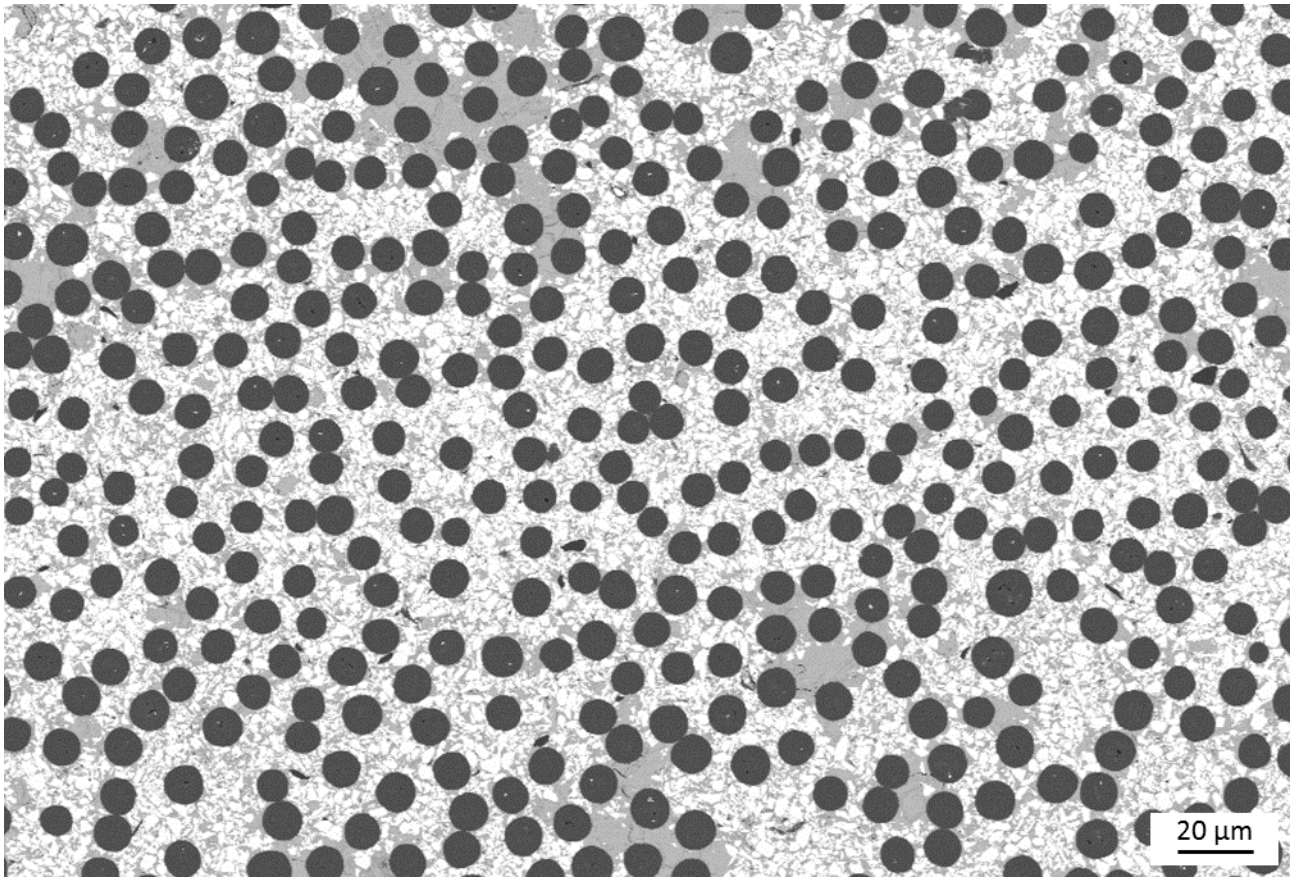


Figure 2. SEM micrograph of the polished section of the 0-0° sample, showing the good homogeneity of carbon fibre (black phase) embedded in  $\text{ZrB}_2$  (white phase) – SiC (grey phase) matrix.

### 3.2 Thermogravimetric analysis

Fig. 3a shows the non-isothermal TG curve up to 1350 °C in air and labels indicate the critical temperatures for the oxidation of the composite. Fig. 3b highlights relevant features of sample surface oxidized after analysis. In Figure 3c, EDS analysis carried out on the red spot (see Fig. 3b) showing the chemical composition of the borosilicate glass.



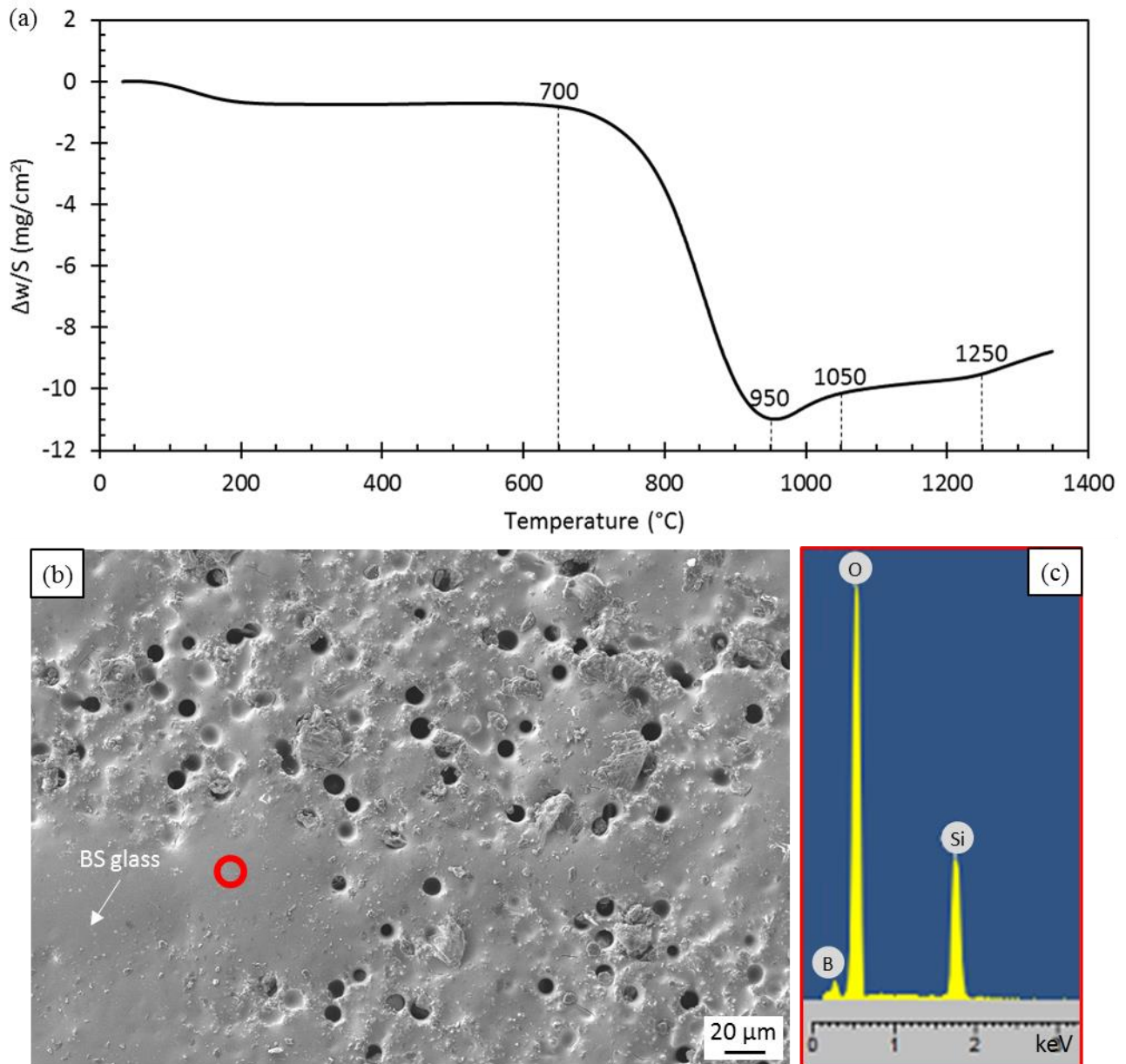
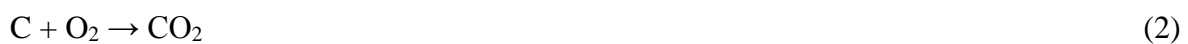


Figure 3. (a) Specific weight change ( $\Delta w/S$ ) vs temperature ( $^{\circ}\text{C}$ ) of the tested material and (b) the SEM micrographs of the oxidized surfaces after TGA, (c) EDS signal of the red spot in (b) showing the chemical composition of the glass.

Above 700  $^{\circ}\text{C}$  and up to 950  $^{\circ}\text{C}$  a rapid weight loss occurred (Fig. 3a). This was ascribed to the rapid oxidation of the exposed carbon fibres due to the evolution of carbon oxides according to the following reactions:



In this range of temperature, the rate of oxidation of  $\text{ZrB}_2$ , see reaction (3), was not sufficient to balance the weight loss due to fibre oxidation. The passivation mechanism promoted by liquid  $\text{B}_2\text{O}_3$  was not sufficient to limit  $\text{O}_2$ -diffusion into the bulk [29].



At 950 °C, mass loss came to a halt. This change in the curve was probably due to an increase in oxidation rate of  $\text{ZrB}_2$  and formation of a partially effective self-protective liquid glass layer percolating in the holes left by fibre removal. Beyond 950 °C and up to 1050 °C, mass gain became predominant. In this range of temperature, the oxidation of polymer derived silicon carbide (pyrolysis at 1000 °C) started to be relevant [35], see reaction (4):



The slope reduction from 1050 to 1250 °C was attributed to the formation of borosilicate glass, see reaction (5), which is more effective to hinder oxygen diffusion. Above 1250 °C a slight increase in the slope pointed out an increase in the rate of oxidation which was attributed to faster  $\text{ZrO}_2$  formation.



### 3.3 Short term oxidation tests

Optical pictures of 0-0°, 0-90° and 2D samples after 1 and 5 min oxidation tests at 1500 and 1650 °C are shown in Fig. 4. After 1 min exposure in air at 1500 °C, the grey colour typical of the as-processed materials acquired blue/dark reflections, index of borosilicate glass formation, and after 5 min, white spots were visible on the surface, indicating the presence of  $\text{ZrO}_2$ . The oxidized samples at 1650 °C for 1 min appeared the most damaged of the series, showing flakes of silica, nevertheless the original shape was preserved, while after 5 min exposure a soft bubble of iridescent glass was formed on the of the samples (Fig. 4d).

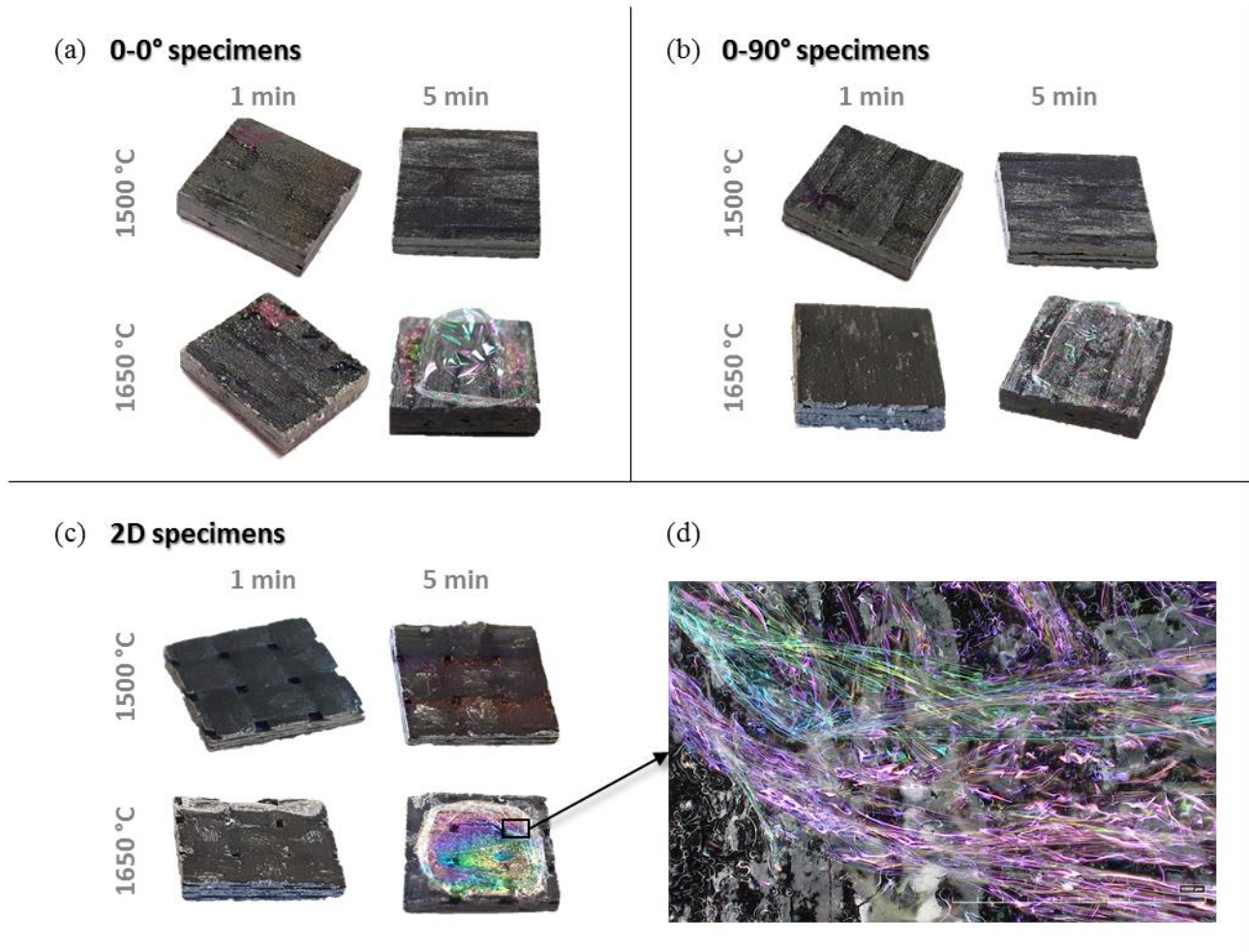


Figure 4. Appearance of the oxidized specimens after bottom loading furnace tests at 1500 and 1650 °C for 1 and 5 min in air: (a) sample 0-0°, (b) sample 0-90° and (c) sample 2D. (d) Optical image detail of a soft iridescent glass bubble grown on the surface of the specimen shown in (c).

A way to evaluate the oxidation extent is the weight change (Table 3). However, it is important to point out that mass changes are the result of negative terms (carbon fibres oxidation and matrix decomposition in volatile species) and positive terms (formation of solid oxide scale).

Although there are remarkable similarities between these materials and those reported in literature, see Table 1, the comparison among mass variations after oxidation tests is not often reliable due to testing conditions (e.g. time and temperature exposure, oxidizing environment, specimen dimensions). In literature, we can often find oxidation test carried out under static air using muffle furnace or thermo-gravimetric analysis (TGA). The bottom loading furnace used to test the oxidation resistance of the composites in this experiment has the advantage to introduce the specimens when the target temperature is reached, avoiding further oxidation during heating ramp.



However, during the introduction of the samples in the furnace, cold air enters the lower part of the chamber, heats up and causes a turbulent flow, leading to harsher conditions than those of a thermogravimetric analyser: Vinci et al. [30] reported that the exposure to air at 1500 °C for 1 min in the bottom loading furnace induced to almost the same degree of oxidation of the equivalent TGA test carried out at 1550 °C for 2.5 h. In addition, the results are often not available or are expressed differently (e.g. weight loss percentage or mass variation normalized over to initial surface). For instance, H. Hu et al. [33] developed C/SiC material enriched with about 25 vol% ZrB<sub>2</sub> particles by PIP and studied the oxidation properties at 1200 °C in a muffle furnace; they reported a mass loss of 4.5% and 11.4% after oxidation for 20 min and 40 min, respectively. D. Huang et al. [36] evaluated the oxidation resistance of C/C-ZrB<sub>2</sub>-ZrC-SiC composite under static air in a muffle furnace at 1100 °C up to 60 min; after 20 min the mass loss was no more than 1%, while after 60 min a mass loss of 10.96 % was reported.

Among sample 0-0°, 0-90° and 2D, the main differences were caused by the greater number of defects and more roughness surface of 2D sample compared the others. Weight loss was notably higher at 1650 °C than at 1500 °C. However, after an initial weight loss, the protective film acted as a barrier and the weight was nearly unchanged after 5 min exposure in air for all of the samples both at 1500 and 1650 °C (Table 3).

Vinci et al. [30] reported a range of weight loss from -1.9 to -3.6 mg/cm<sup>2</sup> testing similar materials in the same furnace at 1500 °C for 1 min. It is interesting to note that despite the content of ZrB<sub>2</sub> was great than 46 vol%, it was not effective to reduce weight loss.

Table 3. Mass variations normalized to the surface area and average thickness of the oxidized layer after short oxidation tests at 1500 and 1650 °C for 1 and 5 min of samples 0-0°, 0-90° and 2D.

	Exposure time (min)	Sample label		
		0-0°	0-90°	2D
$\Delta m/S$ 1500 °C (mg/cm <sup>2</sup> )	1	-2.9	-3.1	-5.1
	5	-1.6	-2.9	-4.9
$\Delta m/S$ 1650 °C (mg/cm <sup>2</sup> )	1	-11.6	-10.7	-7.6
	5	-12.3	-10.1	-8.3

Oxide thickness 1500 °C (μm)	1	~20	~21	~27
	5	~26	~26	~40
Oxide thickness 1650 °C (μm)	1	~30	~30	~43
	5	~32	~33	~46

---

In the following, the crystalline phases of tested samples were discussed. As example, in Fig. 5, X-ray diffraction patterns collected on the surface of the 0-0° specimens, after oxidation in air at 1500 and 1650 °C for 1 and 5 min, were reported. The main crystalline phase was monoclinic ZrO<sub>2</sub> (PDF 65-1025) as product of oxidation of ZrB<sub>2</sub> phase, that increased with the increase of time and oxidation temperature; trace amounts of tetragonal zirconia (PDF 88-1007) was recognized only in XRD patterns after oxidation at 1500 °C. B<sub>2</sub>O<sub>3</sub> was not detected in the surface layer; this could be attributed to its relatively low melting temperature (445 °C) [37] which leads to the formation of a glass. SiC(O) evolution was more difficult to track because during its surficial oxidation into glassy and crystalline SiO<sub>2</sub> (PDF 47-11449) [38], the underlying SiC(O) was subjected to crystallization into β-SiC (PDF 65-0360). Moreover, the crystallinity of SiC increased with the increase of the oxidation temperature and exposure time. No reflections relative to carbon or carbides were observed for all the oxidized specimens. For all the oxidized composites peaks relative to ZrB<sub>2</sub> were still well visible. On the contrary, Vinci et al. [30] did not observed ZrB<sub>2</sub> reflections after oxidation of C/ZrB<sub>2</sub>-SiC at 1500 and 1650 °C despite the initial higher content of ZrB<sub>2</sub> in the matrix, see Table 1. XRD patterns of samples 0-90° and 2D are not shown because there were no significant differences.

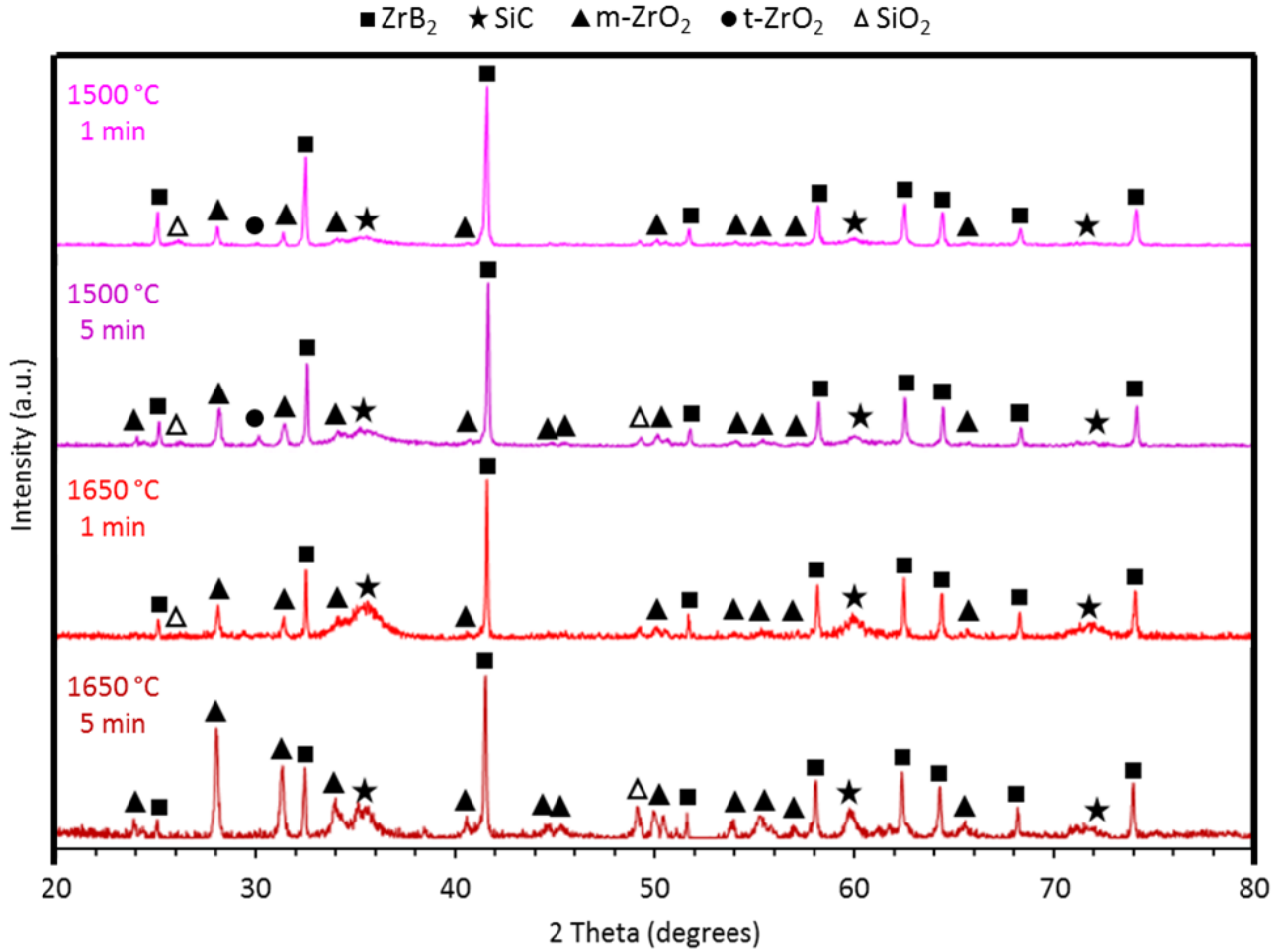


Figure 5. X-ray diffraction patterns collected on the surface of 0-0° specimens after oxidation at 1500 and 1650 °C in air for 1 and 5 min.

Following the XRD investigation, SEM-EDS characterization was carried out on the surface and cross section of the oxidized samples. A typical top view of the surface of the specimens oxidized at 1500 and 1650 °C for 1 and 5 min is shown in Fig. 6a-d, insets in Figures highlight the evolution of morphology of ZrO<sub>2</sub> grains increasing time and temperature of the oxidation test.

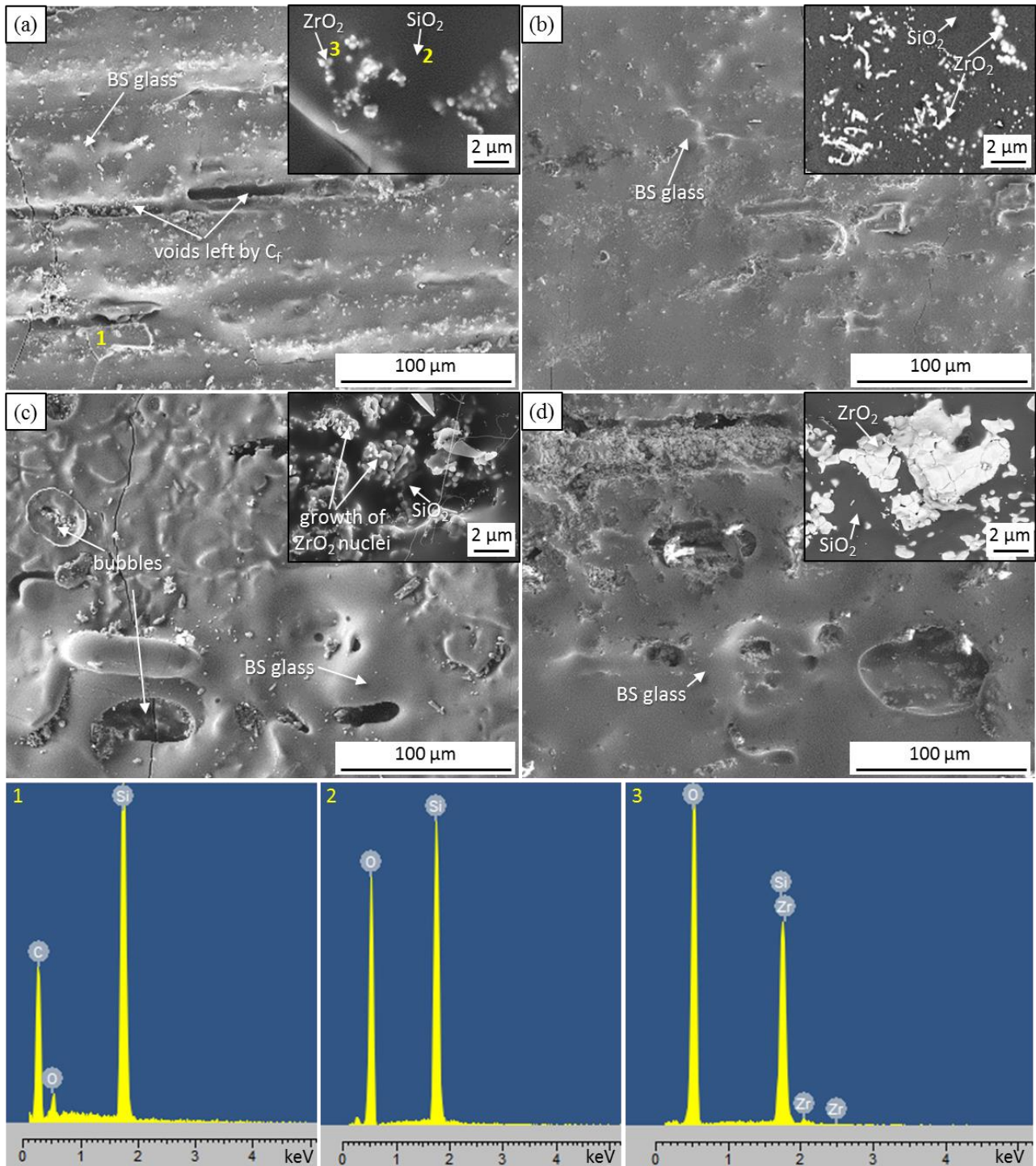


Figure 6. Top view of specimens (0-0° sample) oxidized in air in a bottom load furnace: at 1500 °C for (a) 1 min and (b) 5 min; at 1650 °C for (c) 1 min and (d) 5 min. Insets of the figures highlight the morphology of ZrO<sub>2</sub> grains embedded in the glass. In the bottom EDS spectra of the phases as indicated.

As can be seen in Fig. 6a, after oxidation at 1500 °C for 1 min fibres onto or close to the surface were consumed and grooves are visible in their place. Tiny precipitated ZrO<sub>2</sub> crystals (bright phase) were found immersed into a borosilicate (BS) glass layer formed on the top. Oxidation at 1500 °C for 5 min induced the formation of a continuous BS glass scale which covered

homogeneously the external surface flowing in the grooves left by oxidized fibre, thus preventing further oxygen penetration inside the material (Fig. 6b). After oxidation at 1650 °C the surface appeared more damaged, a higher amount of blisters was observed and the whole surface became rougher (Fig. 6c,d). The great amount of liquid phase which spread from the subsurface towards the surface and the evolution of volatile oxides formed during oxidation led to bubble formation and explosion. It caused the exposure to oxygen of the underlying bulk layer [30,39]. Further inspection on the ruptured bubbles showed islands of tiny  $\text{ZrO}_2$  crystals in coral-like shape, in agreement with [30] (inset in Fig. 6c), due to the evolution of small nuclei in branches of a dendrite. Previously Karlsdottir et al. [40] called this type of dendritic zirconia as “secondary zirconia” and reported that it is dissolved in the oxide boron–silica–zirconia liquid, thus crystals precipitated when the  $\text{B}_2\text{O}_3$  evaporates. The number of blisters in the borosilicate glass scale increased with the exposure time at 1650 °C (Fig. 6d), precipitated  $\text{ZrO}_2$  crystals underneath the ruptured bubbles increased in size and took on a rounded shape (inset in Fig. 6d). A top view of the surface of the specimens of samples 0-90° and 2D oxidized at 1500 °C and 1650 °C for 1 and 5 min are not reported because the microstructural features were found very similar to those reported in Fig. 6.

In supplementary information, see Fig. S1, the low magnification micrographs of the cross section of samples 0-0°, 0-90° and 2D after the four oxidation tests are presented. As example, micrographs of the cross section of the oxidized samples 0-0° at 1500 °C for 1 min are reported below in Fig. 7a-e. The several EDS analyses, carried out in different parts of the sample, are numbered. It is difficult to detect  $\text{B}_2\text{O}_3$  by EDS, as boron is a light element [41].

Fig. 7a,b shows the cross section of the sample close to the top surface, which was not grinded after manufacturing to avoid interruption of fibres, while Fig. 7c shows the cross section of the specimen close to a machined side. As can be seen in Fig. 7a, the matrix underneath the top (orange dashed lines) was enriched of  $\text{SiC}(\text{O})$  and  $\text{SiO}_2$  (see EDS spectrum in Fig. 7).

A detail of partially filled holes left by two carbon fibre burned is reported in Fig. 7b. It is worthy to note that  $\text{ZrB}_2$  close to the surface appeared only partially oxidized, showing nano-crystals of  $\text{ZrO}_2$



on the particle surface (Fig. 7c). In the cross section of a machined side (Fig. 7d), it is easier to evaluate the thickness of the oxide scale. Hence, the modified layer thickness of the specimen was found in the range of 5-25  $\mu\text{m}$ . Moving inwards in the oxidized scale, it was also possible to see a carbon fibre partially surrounded by BS glass film containing inclusions of  $\text{ZrO}_2$ , that could be considered a further mechanism of fibre protection toward oxidation (Fig. 7e).

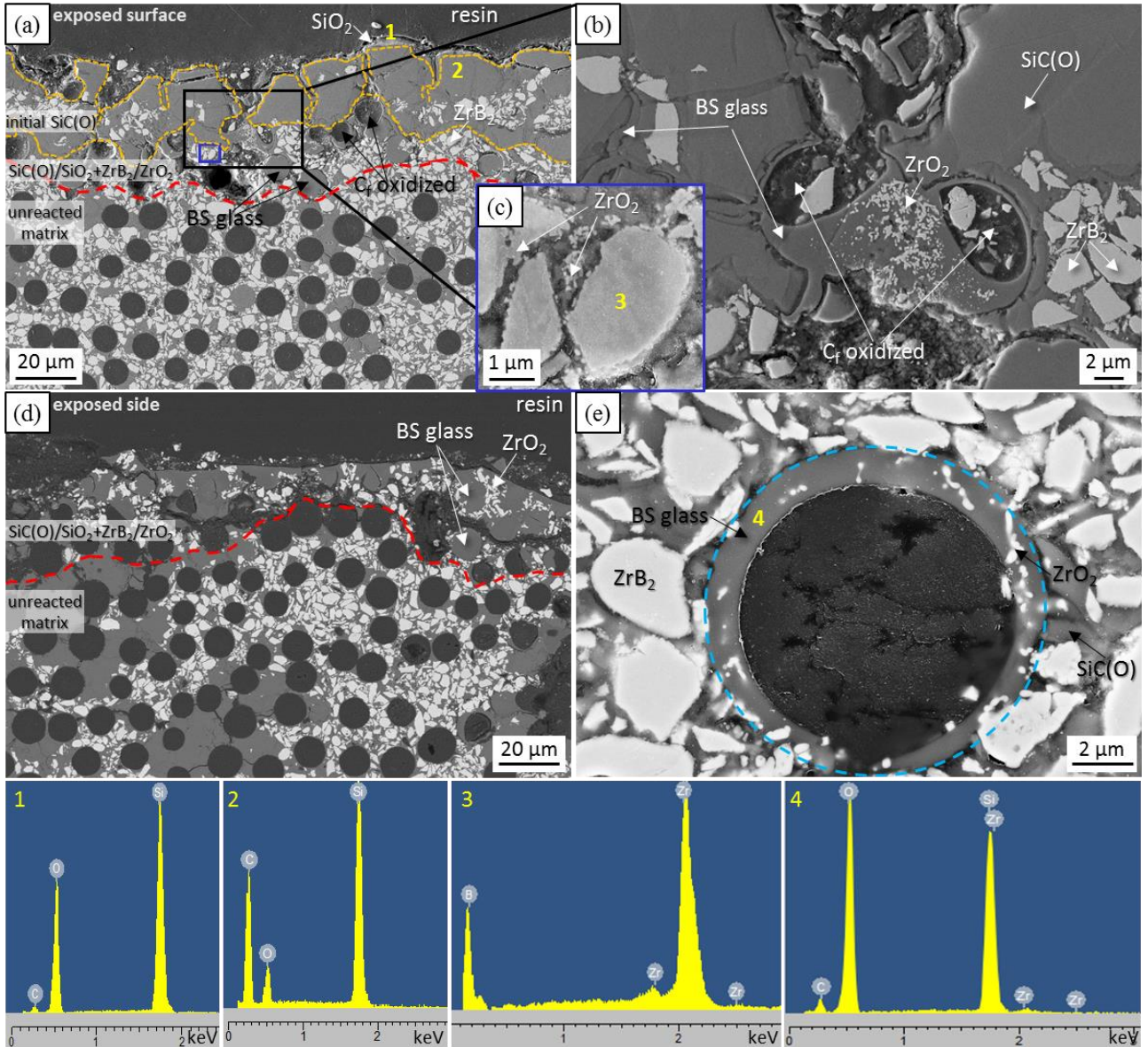


Figure 7. Polished cross section of the specimen (sample 0-0°) after short term oxidation test at 1500 °C for 1 min in air. (a) Micrograph of the exposed surface,  $\text{SiC(O)}$ -rich area, (b) magnification of the BS glass in the voids left by the  $\text{C}_f$  oxidation and (c) magnification of the partially oxidized  $\text{ZrB}_2$  particles; (d) micrograph of the exposed side. (e) High magnification micrograph of a fibre where the oxidation stopped thanks to the BS glass (marked with blue circle) that surrounded it. In the bottom EDS spectra of the phases as numbered.

The morphology of the cross section after 5 min exposure at 1500 °C is shown in Fig. 8a-c. The outer part was composed by a compact scale of BS glass and solid inclusions ( $\text{ZrO}_2$ ) with a

thickness of  $\sim 26 \mu\text{m}$  (Fig. 8a). Despite the thickness of oxide scale was found similar to the shorter oxidation test, the prolonged time of exposure to oxygen caused the almost completely conversion of surficial  $\text{SiC}(\text{O})$  into  $\text{SiO}_2$  and later into BS glass due to reaction with  $\text{B}_2\text{O}_3$ . High magnification micrographs showed many protuberances consisting of a core of fine secondary  $\text{ZrO}_2$  surrounded by glass [40] (Fig. 8b) and the progressive oxidation of  $\text{ZrB}_2$  particles from the external surface towards the unreacted matrix (Fig. 8c).

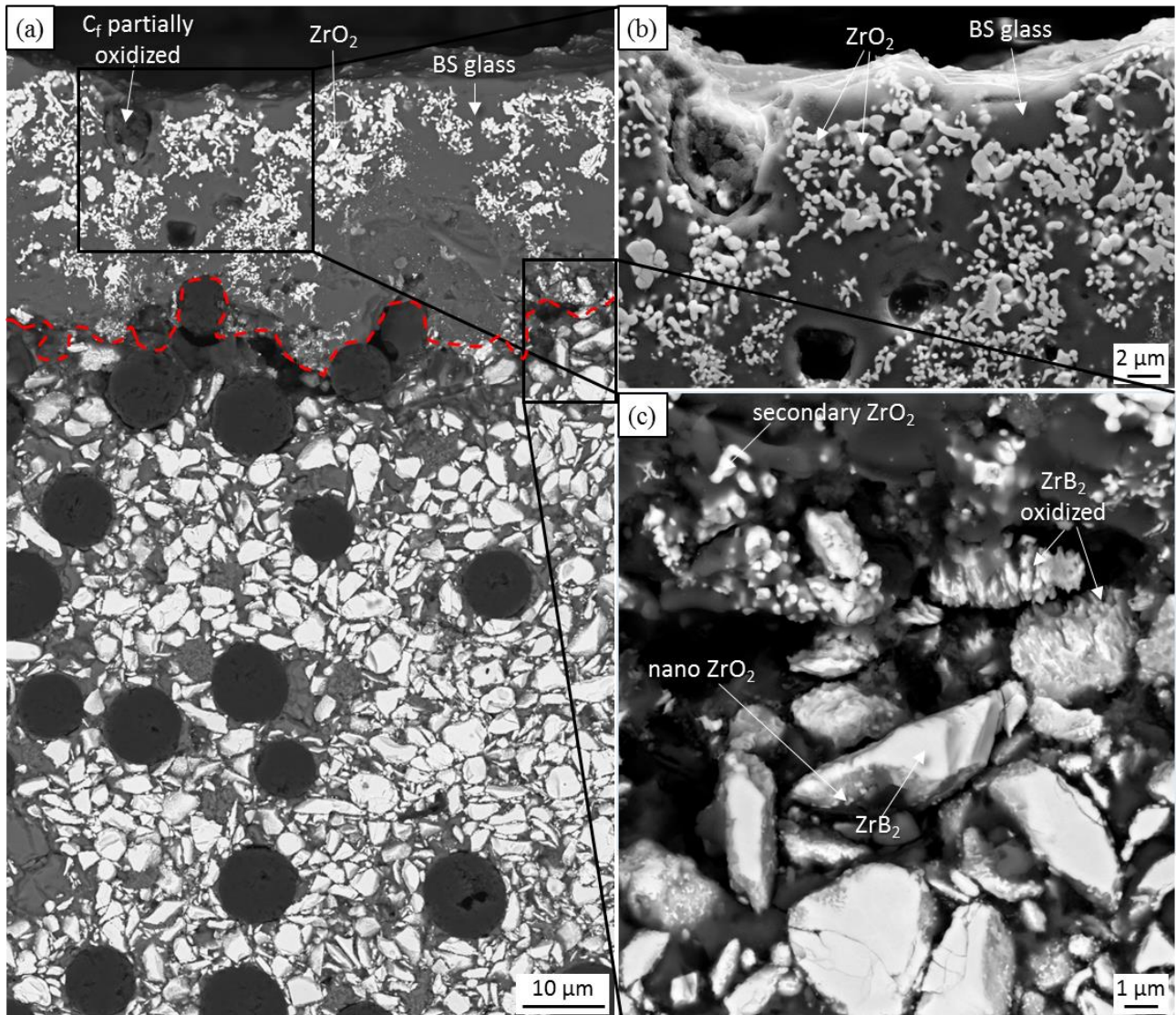


Figure 8. Polished cross section of specimen (sample 0-0°) after short term oxidation test at 1500 °C for 5 min in air: (a) overview of the microstructure, (b) magnification of the BS glass in which secondary  $\text{ZrO}_2$  precipitates are embedded and (c) detail of  $\text{ZrB}_2$  particles and progressive oxidation to  $\text{ZrO}_2$  moving towards the top.

The microstructure of sample cross section after oxidation at 1650 °C for 1 min is visible in Fig. 9a-d. In Fig. 9a a layered structure is visible: an external borosilicate glass scale, an intermediate layer of  $\text{ZrO}_2/\text{SiO}_2$  and an unreacted matrix layer. The coarsening of  $\text{ZrO}_2$  grains is visible in Fig. 9b. A SiC-depleted layer between the  $\text{ZrO}_2/\text{SiO}_2$  scale and the unreacted matrix was not detected. That region is commonly found in oxidized  $\text{ZrB}_2\text{-SiC}$  bulk ceramics, because of the active oxidation of SiC to volatile SiO [14,39]. Rezaie et al. [42] studied that graphite addition in a  $\text{ZrB}_2/\text{SiC}$  ceramic may affect the formation of this layer, as it promotes the preferential formation of  $\text{CO}_{(\text{g})}$ . Hence, the lack of SiC-depleted region very likely depends on the high carbon fibre content. In Fig. 9c is reported a SiC(O)-rich area, the matrix damage was higher, got right into a depth of about 55  $\mu\text{m}$ . This observation is in agreement with ref. [43], cracked surficial SiC(O) acted as a preferential channel for transport of the  $\text{O}_2$  through the composite. Such SiC(O)-rich areas were found more prevalent in the sample 2D, see Fig. 1d compared to samples 0-0° and 0-90°. For the sake of comparison, in Fig. 9d, a cross section highlighting the lateral view of the fibres is shown. The micrograph froze the dynamics of two opposite mechanisms: the glass that tries to fill the channels and the gases that try to escape. The oxidized thickness was calculated to be about 90 - 150  $\mu\text{m}$ .



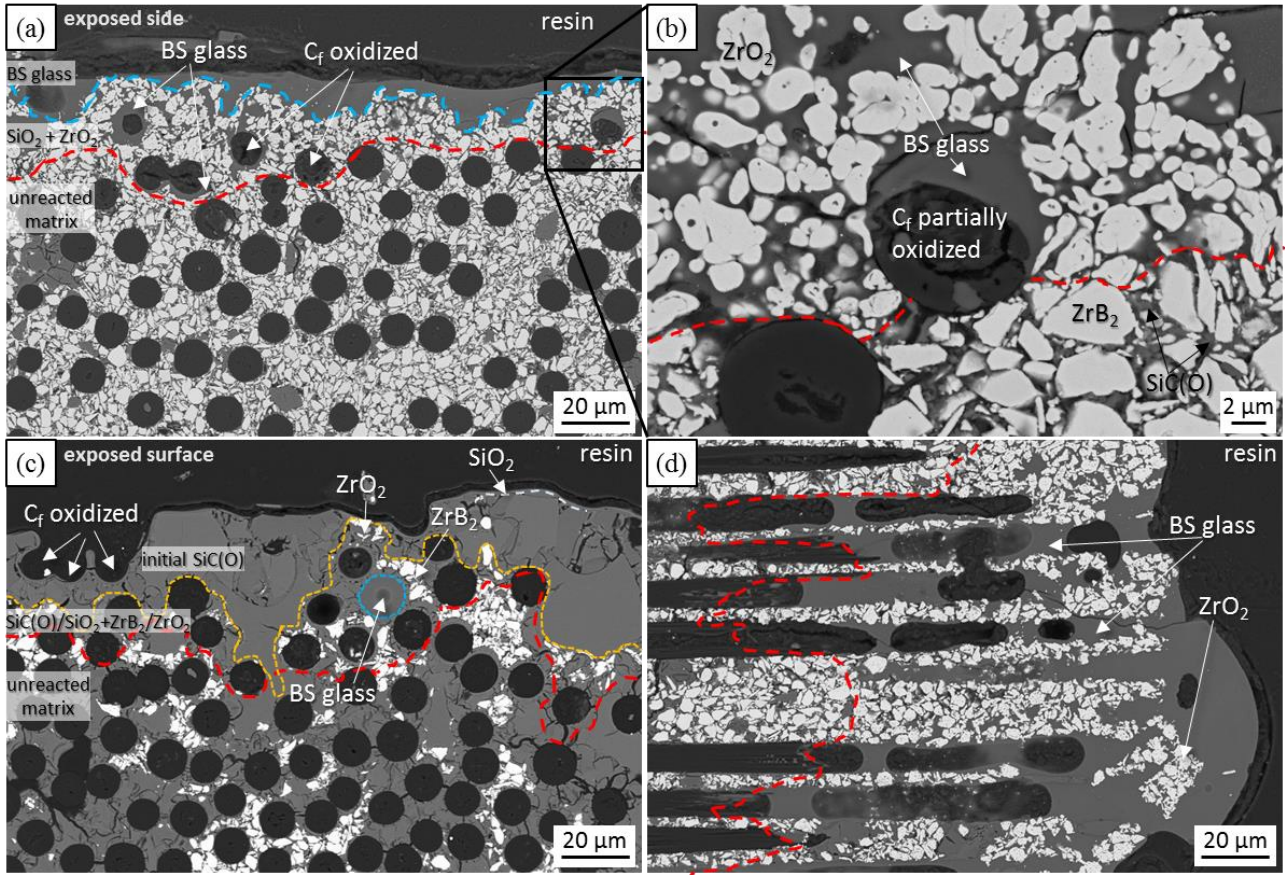


Figure 9. Polished cross section of specimen (sample 0-0°) after short term oxidation test at 1650 °C for 1 min in air: (a) micrograph of the exposed surface in a ZrB<sub>2</sub>-rich area and (b) magnification of a partially oxidized fibre beneath the surface and the void filled by the BS glassy phase, (c) micrograph of the exposed surface in a SiC(O)-rich area, (d) lateral view of fibres.

The same microstructural features were observed after oxidation at 1650 °C for 5 min in air (Fig. 10a-e). A low magnification micrograph (Fig. 10a) demonstrated an optimal resistance after 5 min exposure, the specimens were not severely attacked by erosion. The function of the borosilicate glass was evident in oxidized sections of the air exposed side (Fig. 10b): the oxide thickness was around 25-35 μm, see average thickness in Table 3. Similarly to what was seen above (Fig. 9a,c), in regions with a higher amount of SiC(O), e.g. top of the specimens, the modified layer was higher, up to 75 μm. In addition, the formation of a large BS glass bubble owing to the vigorous gas escape was reported in Fig. 10c. Partially attacked matrix and fibres were found underneath the oxide scale (Fig. 10d) and fully non oxidized bulk matrix and C<sub>f</sub> (Fig. 10e) were reported to highlight the difference in microstructure.

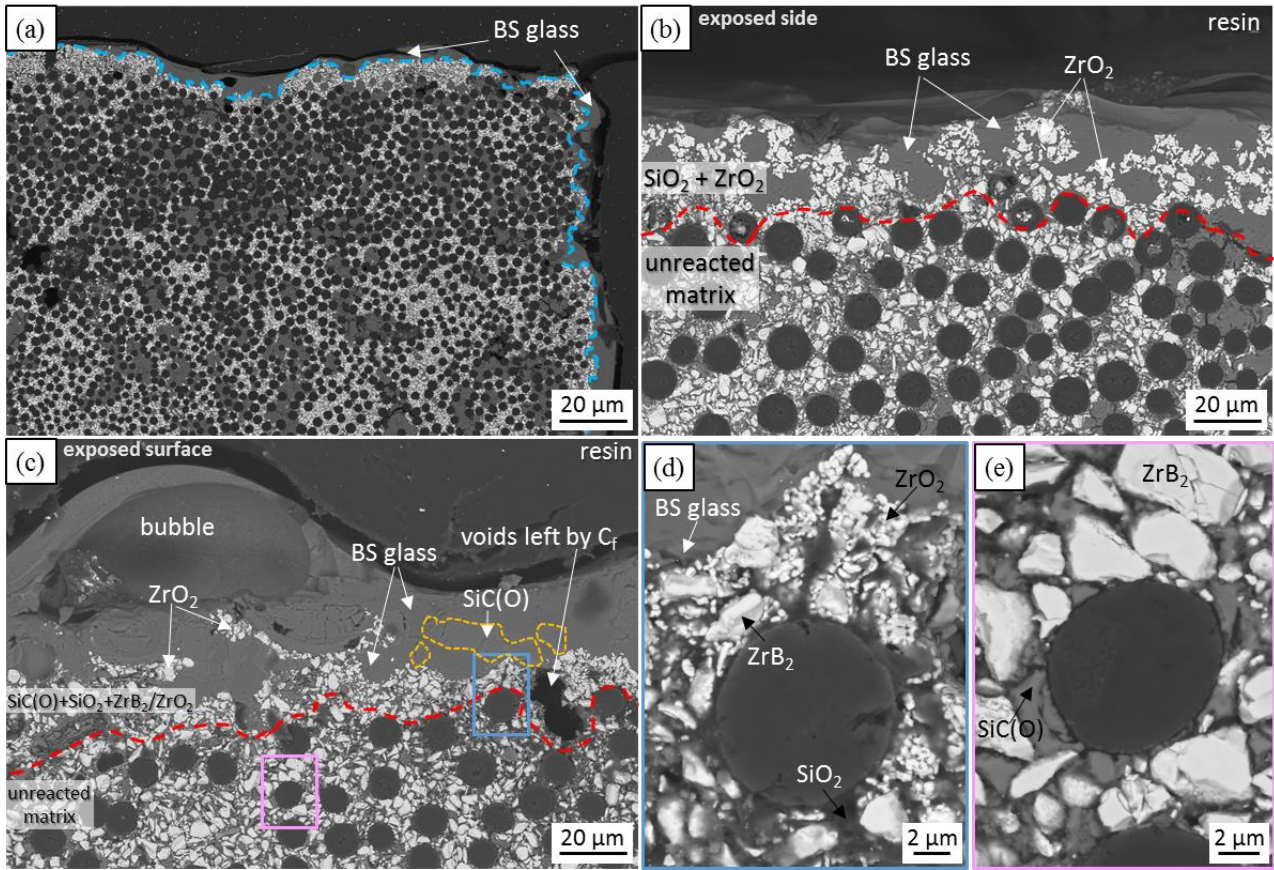


Figure 10. Polished cross section of specimen (sample 0-0°) after short term oxidation test at 1650 °C for 5 min in air: (a) low magnification micrograph of an edge exposed to air flow, (b) micrograph of the exposed surface in a ZrB<sub>2</sub>-rich area and (c) micrograph of the exposed surface in a SiC(O)-rich area, showing oxidized thicknesses; high magnification micrographs of a fibre underneath the exposed surface surrounded by: a partially oxidized matrix (d), unreacted matrix (e).

In the supplementary information, Fig. S2, are reported the cross section of specimens (sample 0-0°) after the four oxidation tests at the same magnification to have a comparison of the different oxide scale thickness in a glance.

Based on the above analysis, the main phenomena occurring during exposition of C/ZrB<sub>2</sub>-SiC were: oxidation of carbon fibres onto or close to the surface, oxidation of ZrB<sub>2</sub> to zirconia and boron oxide, oxidation of SiC to silica, formation of a borosilicate glass [29,30,32]. As described before, samples were introduced inside the hot chamber when the target temperature was reached, i.e. 1500 and 1650 °C. Opening the furnace the temperature slightly decreased, but in a few tens of seconds the temperature was re-stabilized. Thus, all oxidation phenomena occurred almost simultaneously. Although the permanence in the critical temperature range (700-1200 °C) [29] was rather short, near-surface fibres were still oxidized rapidly, and this contributed to an initial weight loss of



material. In our opinion, the weight losses observed was not justified by the thin layer of oxide scale observed. The explanation could be due to the conversion of SiC(O) matrix into crystalline SiC, as it was obtained at the relatively mild condition of 1000 °C. Indeed, polymer-derived SiC(O) often contains free turbostratic carbon and terminal Si-CH<sub>3</sub> and Si-OH groups in case of incomplete pyrolysis [44]. Moreover, oxygen in polymer-derived SiC(O) reacts with carbon causing mass loss decomposing into SiO and CO gases via reaction 6 [45].



According to the microstructural features of the specimens, the main mechanisms occurring in the UHTCMCs containing ZrB<sub>2</sub> particles embedded in amorphous SiC(O) are sketched in Fig. 11.

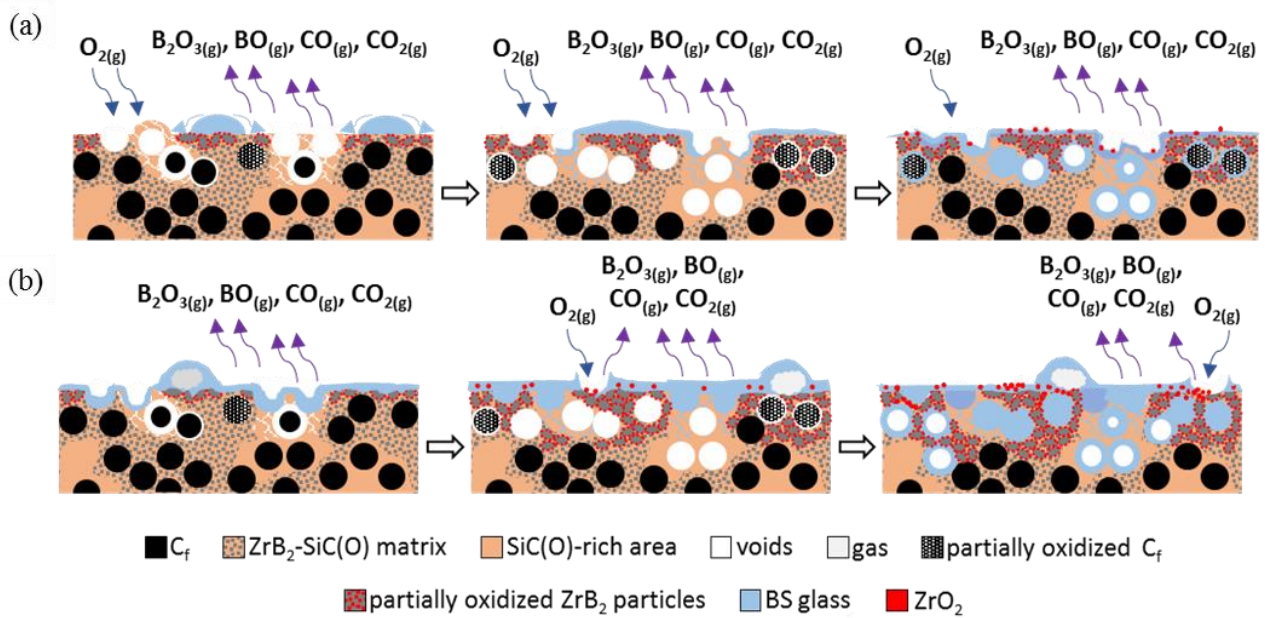


Figure 11. Sketch of oxidation mechanism of C<sub>f</sub>/ZrB<sub>2</sub>-SiC fabricated by water-based ZrB<sub>2</sub> powder slurry infiltration followed by 6 PIP cycles at (a) 1500 °C and (b) 1650 °C.

Yang et al. studied and comprehensively discussed the evolution of microstructure and properties of C/SiC composites prepared by PIP process after high-temperature oxidation. After oxidation in air at 1500 °C, the C/SiC composites were severely damaged, carbon fibres oxidation and many microcracks emerged [4]. The same author tested PIP-C/SiC at 1600 °C, the carbon fibres were completely consumed and SiC matrix became loose due to the escape of the gas phases

produced beneath the surface [5]. The results obtained here indicate that the addition of  $\text{ZrB}_2$  particles through a first cycle of slurry infiltration was essential for the formation of a borosilicate glassy layer, which played an important role in closing the holes left by carbon fibres oxidation and the cracks in the surface and subsurface layer.

It is interesting to compare the performance of the three samples analysed in this work with samples reported in ref [31] and [32]. To this aim, the plot of Fig. 12a shows the oxide scale thickness after oxidation tests and carbon fibre content of samples while the plot of Fig. 12b shows density and the relative amounts of  $\text{ZrB}_2$ , SiC,  $\text{C}_f$  and porosity (normalized values) of samples. It can be clearly seen that from sample 0-0° to ZS10-55F the oxidation resistance is not strictly correlated to the increase of fibre content. However, in the case of sample Z40S-55F the amount of fibres (55 vol%) was too high to have a uniform coating by the matrix, resulting in poor resistance to oxidation, moreover the sample presents large  $\text{ZrB}_2$ -free matrix intra-bundle zones. The overall amount of SiC in the composite is also important to passivate the material surface. In samples Z10S-40F the presence of 6 vol% SiC favoured the formation of a borosilicate glass that diffused across the scale but efficacy is lower than in case of sample ZS20 and all of the samples of this work.

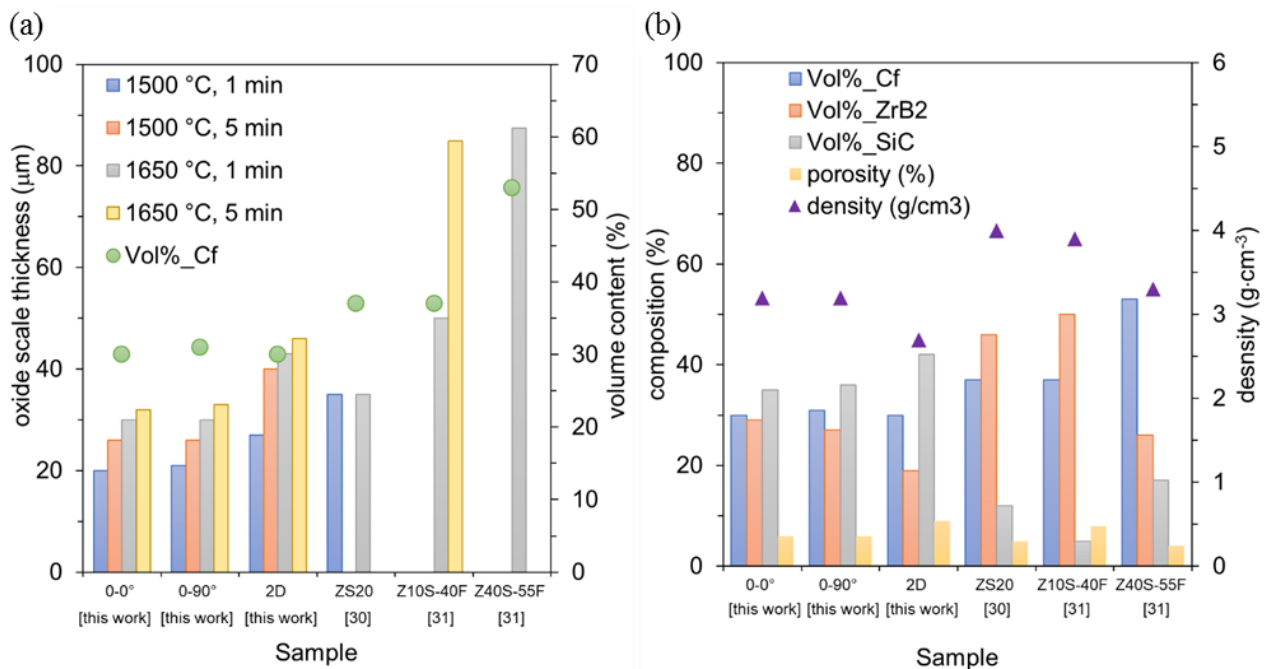


Fig. 12. Plots show (a) the volumetric content of fibre (Vol%<sub>Cf</sub>) of samples and the thickness of the oxide scale after tests, (b) density and relative amounts of ZrB<sub>2</sub>, SiC, C<sub>f</sub> and porosity (normalized values) of the three samples of this work and three samples of ref. [30] and [31]. Unpublished data of the oxide scale thickness after tests at 1650 °C were reported for samples ZS10-40F and ZS40S-55F.

## 4. Conclusions

The oxidation behaviour of C<sub>f</sub>/ZrB<sub>2</sub>-SiC with different fibre architecture, manufactured by ZrB<sub>2</sub> powder slurry impregnation followed by SMP-10 infiltration and mild pyrolysis at 1000 °C, was investigated via TGA up to 1350 °C. The capability of the material to withstand the extreme harsh conditions was evaluated via short term oxidation tests in air at 1500 and 1650 °C in a bottom loading furnace for 1 and 5 min. The exposure to high temperature in air activated the formation of a borosilicate glass, typical of ZrB<sub>2</sub>-SiC binary systems, a content of ZrB<sub>2</sub> about 20-30 vol% of the matrix is able to impart a fast passivation. As expected, the oxidation resistance was affected by the distribution of ZrB<sub>2</sub> into the SiC matrix, highlighting the direct correlation between thickness of oxide scale and goodness of slurry infiltration process. Independently of fibre architecture complexity the material hindered the oxygen penetration within 5 min.

## Data availability statement

All data included in this study are available upon request by contact with the corresponding author.

## Credit authorship contribution statement

F. Servadei: Investigation, Formal analysis, Data curation, Writing - original draft. L. Zoli: Conceptualization, Supervision, Methodology. A. Vinci: Writing - review & editing. P. Galizia: Supervision. D. Sciti: Project administration, Funding acquisition, Supervision, Writing - review & editing.

## Declaration of Competing Interests

We declare that we have no financial and personal relationships with other people or organizations that can inappropriately influence our work, there is no professional or other personal interest of any nature or kind in any product, service and/or company that could be construed as influencing the position presented in, or the review of, the manuscript entitled “Significant improvement of the self-protection capability of ultra-high temperature ceramic matrix composites”.

## Acknowledgements

The authors wish to thank A. Piancastelli, A. Natali Murri and C. Capiani for mercury intrusion porosimetry, thermogravimetric analysis and X-ray diffraction analysis, respectively.

This work was supported by the European Union’s Horizon 2020 “Research and innovation programme” [grant agreement No 685594].

## Appendix A. Supplementary data

The following is Supplementary data to this article:

Download : Download Word document (809KB)

## References

- [1] W. Krenkel, Ceramic Matrix Composites, Wiley-VCH, Weinheim, 2008.  
<https://doi.org/10.1002/9783527622412>.
- [2] S. Kumar, K.C. Shekar, B. Jana, L.M. Manocha, N. Eswara Prasad, C/C and C/SiC Composites for Aerospace Applications, in: N. Eswara Prasad, R. Wanhill (Eds.), *Aerosp. Mater. Mater. Technol. Vol. 1 Aerosp. Mater. Indian Inst. Met. Ser.*, Springer, Singapore, Singapore, 2017: pp. 343–369. [https://doi.org/10.1007/978-981-10-2134-3\\_15](https://doi.org/10.1007/978-981-10-2134-3_15).
- [3] B. Heidenreich, C/SiC and C/C-SiC Composites, in: P.B. Narottam, J. Lamon (Eds.), *Ceram. Matrix Compos.*, John Wiley & Sons, Inc., Hoboken, NJ, USA, 2014: pp. 147–216.  
<https://doi.org/10.1002/9781118832998.ch6>.
- [4] Y. Xiang, W. Li, S. Wang, Z.H. Chen, Oxidation behavior of oxidation protective coatings

for PIP-C/SiC composites at 1500 °C, *Ceram. Int.* 38 (2012) 9–13.

<https://doi.org/10.1016/j.ceramint.2011.06.063>.

- [5] X. Yang, C. Feng, Z. hang Peng, W. Yi, G. de Li, Evolution of microstructure and mechanical properties of PIP-C/SiC composites after high-temperature oxidation, *J. Asian Ceram. Soc.* 5 (2017) 370–376. <https://doi.org/10.1016/j.jascer.2017.07.001>.
- [6] Y. Wang, Z. Chen, S. Yu, Ablation behavior and mechanism analysis of C/SiC composites, *J. Mater. Res. Technol.* 5 (2016) 170–182. <https://doi.org/10.1016/j.jmrt.2015.10.004>.
- [7] Y. Cui, A. Li, B. Li, X. Ma, R. Bai, W. Zhang, M. Ren, J. Sun, Microstructure and ablation mechanism of C/C-SiC composites, *J. Eur. Ceram. Soc.* 34 (2014) 171–177. <https://doi.org/10.1016/j.jeurceramsoc.2013.08.026>.
- [8] B. Yan, Z. Chen, J. Zhu, J. Zhang, Y. Jiang, Effects of ablation at different regions in three-dimensional orthogonal C/SiC composites ablated by oxyacetylene torch at 1800 °C, *J. Mater. Process. Technol.* 209 (2009) 3438–3443. <https://doi.org/10.1016/j.jmatprotec.2008.08.002>.
- [9] S. Tang, J. Deng, S. Wang, W. Liu, K. Yang, Ablation behaviors of ultra-high temperature ceramic composites, *Mater. Sci. Eng. A.* 465 (2007) 1–7. <https://doi.org/10.1016/j.msea.2007.02.040>.
- [10] A. Cecere, R. Savino, C. Allouis, F. Monteverde, Heat transfer in ultra-high temperature advanced ceramics under high enthalpy arc-jet conditions, *Int. J. Heat Mass Transf.* 91 (2015) 747–755. <https://doi.org/10.1016/j.ijheatmasstransfer.2015.08.029>.
- [11] M.M. Opeka, I.G. Talmy, E.J. Wuchina, J.A. Zaykoski, S.J. Causey, Mechanical, Thermal, and Oxidation Properties of Refractory Hafnium and zirconium Compounds, *J. Eur. Ceram. Soc.* 19 (1999) 2405–2414. [https://doi.org/10.1016/S0955-2219\(99\)00129-6](https://doi.org/10.1016/S0955-2219(99)00129-6).
- [12] S.R. Levine, E.J. Opila, M.C. Halbig, J.D. Kiser, M. Singh, J.A. Salem, Evaluation of ultra-high temperature ceramics for aeropropulsion use, *J. Eur. Ceram. Soc.* 22 (2002) 2757–2767. [https://doi.org/10.1016/S0955-2219\(02\)00140-1](https://doi.org/10.1016/S0955-2219(02)00140-1).

- [13] A.L. Chamberlain, W.G. Fahrenholtz, G.E. Hilmas, D.T. Ellerby, Characterization of zirconium diboride for thermal protection systems, *Key Eng. Mater.* 264–268 (2004) 493–496. <https://doi.org/10.4028/www.scientific.net/kem.264-268.493>.
- [14] W.G. Fahrenholtz, G.E. Hilmas, I.G. Talmy, J.A. Zaykoski, Refractory diborides of zirconium and hafnium, *J. Am. Ceram. Soc.* 90 (2007) 1347–1364. <https://doi.org/10.1111/j.1551-2916.2007.01583.x>.
- [15] W.G. Fahrenholtz, G.E. Hilmas, A.L. Chamberlain, J.W. Zimmermann, B. Fahrenholtz, Processing and characterization of ZrB<sub>2</sub>-based ultra-high temperature monolithic and fibrous monolithic ceramics, in: *J. Mater. Sci.*, Springer, 2004: pp. 5951–5957. <https://doi.org/10.1023/B:JMSC.0000041691.41116.bf>.
- [16] A. Rezaie, W.G. Fahrenholtz, G.E. Hilmas, Evolution of structure during the oxidation of zirconium diboride-silicon carbide in air up to 1500 °C, *J. Eur. Ceram. Soc.* 27 (2007) 2495–2501. <https://doi.org/10.1016/j.jeurceramsoc.2006.10.012>.
- [17] W.G. Fahrenholtz, Thermodynamic analysis of ZrB<sub>2</sub>-SiC oxidation: Formation of a SiC-depleted region, *J. Am. Ceram. Soc.* 90 (2007) 143–148. <https://doi.org/10.1111/j.1551-2916.2006.01329.x>.
- [18] G. Hilmas, W. Fahrenholtz, A. Chamberlain, D. Ellerby, Oxidation of ZrB<sub>2</sub>-SiC Ceramics under Atmospheric and Reentry Conditions, *Undefined*. (2005).
- [19] E. Zapata-Solvas, D.D. Jayaseelan, P.M. Brown, W.E. Lee, Effect of La<sub>2</sub>O<sub>3</sub> addition on long-term oxidation kinetics of ZrB<sub>2</sub>-SiC and HfB<sub>2</sub>-SiC ultra-high temperature ceramics, *J. Eur. Ceram. Soc.* 34 (2014) 3535–3548. <https://doi.org/10.1016/j.jeurceramsoc.2014.06.004>.
- [20] A. Paul, S. Venugopal, J.G.P. Binner, B. Vaidhyanathan, A.C.J. Heaton, P.M. Brown, UHTC-carbon fibre composites: Preparation, oxyacetylene torch testing and characterisation, *J. Eur. Ceram. Soc.* 33 (2013) 423–432. <https://doi.org/10.1016/j.jeurceramsoc.2012.08.018>.
- [21] L. Silvestroni, D. Sciti, Densification of ZrB<sub>2</sub>-TaSi<sub>2</sub> and HfB<sub>2</sub>-TaSi<sub>2</sub> Ultra-High-Temperature Ceramic Composites, *J. Am. Ceram. Soc.* 94 (2011) 1920–1930.



<https://doi.org/10.1111/j.1551-2916.2010.04317.x>.

- [22] S. Zhu, W.G. Fahrenholtz, G.E. Hilmas, Influence of silicon carbide particle size on the microstructure and mechanical properties of zirconium diboride-silicon carbide ceramics, *J. Eur. Ceram. Soc.* 27 (2007) 2077–2083. <https://doi.org/10.1016/j.jeurceramsoc.2006.07.003>.
- [23] K.S. Cissel, E. Opila, Oxygen diffusion mechanisms during high-temperature oxidation of  $\text{ZrB}_2$ -SiC, *J. Am. Ceram. Soc.* 101 (2018) 1765–1779. <https://doi.org/10.1111/jace.15298>.
- [24] H. Zhou, L. Gao, Z. Wang, S. Dong,  $\text{ZrB}_2$ -SiC Oxidation Protective Coating on C/C Composites Prepared by Vapor Silicon Infiltration Process, *J. Am. Ceram. Soc.* 93 (2010) 915–919. <https://doi.org/10.1111/j.1551-2916.2009.03481.x>.
- [25] O. Haibo, L. Cuiyan, H. Jianfeng, C. Liyun, F. Jie, L. Jing, X. Zhanwei, Self-healing  $\text{ZrB}_2$ - $\text{SiO}_2$  oxidation resistance coating for SiC coated carbon/carbon composites, *Corros. Sci.* 110 (2016) 265–272. <https://doi.org/10.1016/j.corsci.2016.04.040>.
- [26] E.L. Corral, R.E. Loehman, Ultra-high-temperature ceramic coatings for oxidation protection of carbon-carbon composites, *J. Am. Ceram. Soc.* 91 (2008) 1495–1502. <https://doi.org/10.1111/j.1551-2916.2008.02331.x>.
- [27] S. Tang, J. Deng, S. Wang, W. Liu, Fabrication and Characterization of an Ultra-High-Temperature Carbon Fiber-Reinforced  $\text{ZrB}_2$ -SiC Matrix Composite, *J. Am. Ceram. Soc.* 90 (2007) 3320–3322. <https://doi.org/10.1111/j.1551-2916.2007.01876.x>.
- [28] L. Liu, H. Li, W. Feng, X. Shi, K. Li, L. Guo, Ablation in different heat fluxes of C/C composites modified by  $\text{ZrB}_2$ -ZrC and  $\text{ZrB}_2$ -ZrC-SiC particles, *Corros. Sci.* 74 (2013) 159–167. <https://doi.org/10.1016/j.corsci.2013.04.038>.
- [29] A. Vinci, L. Zoli, E. Landi, D. Sciti, Oxidation behaviour of a continuous carbon fibre reinforced  $\text{ZrB}_2$ -SiC composite, *Corros. Sci.* 123 (2017) 129–138. <https://doi.org/10.1016/j.corsci.2017.04.012>.
- [30] A. Vinci, L. Zoli, D. Sciti, Influence of SiC content on the oxidation of carbon fibre reinforced  $\text{ZrB}_2$ /SiC composites at 1500 and 1650 °C in air, *J. Eur. Ceram. Soc.* 38 (2018)

3767–3776. <https://doi.org/10.1016/j.jeurceramsoc.2018.04.064>.

- [31] L. Zoli, D. Sciti, Efficacy of a  $\text{ZrB}_2$ –SiC matrix in protecting C fibres from oxidation in novel UHTCMC materials, *Mater. Des.* 113 (2017) 207–213.  
<https://doi.org/10.1016/j.matdes.2016.09.104>.
- [32] F. Servadei, L. Zoli, P. Galizia, A. Vinci, D. Sciti, Development of UHTCMCs via water based  $\text{ZrB}_2$  powder slurry infiltration and polymer infiltration and pyrolysis, *J. Eur. Ceram. Soc.* 40 (2020) 5076–5084. <https://doi.org/10.1016/j.jeurceramsoc.2020.05.054>.
- [33] H. Hu, Q. Wang, Z. Chen, C. Zhang, Y. Zhang, J. Wang, Preparation and characterization of C/SiC– $\text{ZrB}_2$  composites by precursor infiltration and pyrolysis process, *Ceram. Int.* 36 (2010) 1011–1016. <https://doi.org/10.1016/j.ceramint.2009.11.015>.
- [34] Q. Li, S. Dong, Z. Wang, G. Shi, Fabrication and properties of 3-D Cf/ $\text{ZrB}_2$ –ZrC–SiC composites via polymer infiltration and pyrolysis, *Ceram. Int.* 39 (2013) 5937–5941.  
<https://doi.org/10.1016/j.ceramint.2012.11.074>.
- [35] G. Chollon, Oxidation Behavior of Ceramic Fibers from the Si–C–N–O System and Sub-Systems, *Key Eng. Mater.* 164–165 (1999) 395–398.  
<https://doi.org/10.4028/www.scientific.net/kem.164-165.395>.
- [36] D. Huang, M. Zhang, Q. Huang, L. Wang, K. Tong, Mechanical Property, Oxidation and Ablation Resistance of C/C– $\text{ZrB}_2$ –ZrC–SiC Composite Fabricated by Polymer Infiltration and Pyrolysis with Preform of Cf/ $\text{ZrB}_2$ , *J. Mater. Sci. Technol.* 33 (2017) 481–486.  
<https://doi.org/10.1016/j.jmst.2016.09.003>.
- [37] Y.H. Seong, D.K. Kim, Oxidation behavior of  $\text{ZrB}_2$ –xSiC composites at 1500 °C under different oxygen partial pressures, *Ceram. Int.* 40 (2014) 15303–15311.  
<https://doi.org/10.1016/j.ceramint.2014.07.036>.
- [38] D. Gao, Y. Zhang, J. Fu, C. Xu, Y. Song, X. Shi, Oxidation of zirconium diboride-silicon carbide ceramics under an oxygen partial pressure of 200Pa: Formation of zircon, *Corros. Sci.* 52 (2010) 3297–3303. <https://doi.org/10.1016/j.corsci.2010.06.004>.

- [39] E. Opila, S. Levine, J. Lorincz, Oxidation of ZrB<sub>2</sub>- And HfB<sub>2</sub>-based ultra-high temperature ceramics: Effect of Ta additions, *J. Mater. Sci.* 39 (2004) 5969–5977.  
<https://doi.org/10.1023/B:JMSC.0000041693.32531.d1>.
- [40] S.N. Karlsdottir, J.W. Halloran, A.N. Grundy, Zirconia transport by liquid convection during oxidation of zirconium diboride-silicon carbide, *J. Am. Ceram. Soc.* 91 (2008) 272–277.  
<https://doi.org/10.1111/j.1551-2916.2007.02142.x>.
- [41] P.A. Williams, R. Sakidja, J.H. Perepezko, P. Ritt, Oxidation of ZrB<sub>2</sub>-SiC ultra-high temperature composites over a wide range of SiC content, *J. Eur. Ceram. Soc.* 32 (2012) 3875–3883. <https://doi.org/10.1016/j.jeurceramsoc.2012.05.021>.
- [42] A. Rezaie, W.G. Fahrenholtz, G.E. Hilmas, The effect of a graphite addition on oxidation of ZrB<sub>2</sub>-SiC in air at 1500°C, *J. Eur. Ceram. Soc.* 33 (2013) 413–421.  
<https://doi.org/10.1016/j.jeurceramsoc.2012.09.016>.
- [43] F. Uhlmann, C. Wilhelmi, S. Schmidt-Wimmer, S. Beyer, C. Badini, E. Padovano, Preparation and characterization of ZrB<sub>2</sub> and TaC containing C<sub>f</sub>/SiC composites via Polymer-Infiltration-Pyrolysis process, *J. Eur. Ceram. Soc.* 37 (2017) 1955–1960.  
<https://doi.org/10.1016/j.jeurceramsoc.2016.12.048>.
- [44] G. Chollon, Oxidation behaviour of polymer-derived ceramics, in: P. Colombo and R. Riedel and G. D. Soraru and H.-J. Kleebe (Ed.), *Polym. Deriv. Ceram. From Nano-Structure to Appl.*, DEStech Publications, 2010: pp. 292–308. 978-1-60595-000-6. fhal-01374117f.
- [45] Y. Hasegawa, K. Okamura, Synthesis of continuous silicon carbide fibre - Part 3 Pyrolysis process of polycarbosilane and structure of the products, *J. Mater. Sci.* 18 (1983) 3633–3648.  
<https://doi.org/10.1007/BF00540736>.